1   **A Novel *Tmem119-tdTomato* Reporter Mouse Model for Studying Microglia in the**

2   **Central Nervous System**

3   Chunsheng Ruan[a], Linlin Sun[b], Alexandra Kroshilina[a], Lien Beckers[a], Philip L. De Jager[a],

4   Elizabeth M. Bradshaw[a], Samuel Hasson[c,d], Guang Yang[b], and Wassim Elyaman[a,*]

5

6   [a]Center for Translational and Computational Neuroimmunology, Department of Neurology,

7   Columbia University Medical Center, New York, NY 10032, USA

8   [b]Department of Anesthesiology, Columbia University Medical Center, New York, NY

9   10032, USA

10 [c]Pfizer Inc., Cambridge, MA 02141, USA

11 [d]Amgen, Cambridge, MA 02141, USA

12

13 *Corresponding author at: Center for Translational and Computational Neuroimmunology,

14 Department of Neurology, Columbia University Medical Center, New York, NY 10032, USA.

15 Email address: we2152@cumc.columbia.edu (W. Elyaman)

Abstract

Microglia are resident immune cells of the central nervous system (CNS). The exact role of microglia in the physiopathology of CNS disorders is not clear due to lack of tools to discriminate between CNS resident and infiltrated innate immune cells. Here, we present a novel reporter mouse model targeting a microglia-specific marker (TMEM119) for studying the function of microglia in health and disease. By placing a reporter cassette (GSG-3xFlag-P2A-tdTomato) between the coding sequence of exon 2 and 3'UTR of the *Tmem119* gene using CRISPR/Cas9 technology, we generated a *Tmem119-tdTomato* knock-in mouse strain. Gene expression assay showed no difference of endogenous *Tmem119* mRNA level in the CNS of *Tmem119*$^{tdTomato/+}$ relative to control Wild-type mice. The cells expressing tdTomato- were recognized by immunofluorescence staining using commercially available anti-TMEM119 antibodies. Using immunofluorescence and flow cytometry techniques, tdTomato^{+} cells were detected throughout the CNS, but not in peripheral tissues of adult *Tmem119*$^{tdTomato/+}$ mice. In addition, aging does not seem to influence TMEM119 expression as tdTomato^{+} cells were detectable in the CNS of older mice (300 and 540 days old). Further immunofluorescence characterization shows that the tdTomato^{+} cells were highly colocalized with Iba1^{+} cells (microglia and macrophages) in the brain, but not with NeuN- (neurons), GFAP- (astrocytes) or Olig2- (oligodendrocytes) labeled cells. Moreover, flow cytometry analysis of brain tissues of adult mice demonstrates that the majority of microglial CD45^{low}CD11b^{+} cells (96.6%) are tdTomato positive. Functionally, using a laser-induced injury model, we measured time-lapse activation of tdTomato-labeled microglia by transcranial two-photon microscopy in live *Tmem119*$^{tdTomato/+}$ mice. Taken together, the *Tmem119-tdTomato* reporter mouse model will serve as a valuable tool to specifically study the role of microglia in health and disease.

1. Introduction

Microglia constitute the resident macrophages of the central nervous system (CNS)(Graeber and Streit, 1990), with a panoply of functions including immune surveillance (Hanisch and Kettenmann, 2007), maintenance of neuronal networks (Wu et al., 2015), and injury repair (Colonna and Butovsky, 2017). Microglia are phagocytic cells, and clearance of debris is thought to be a key function, especially in aging (Pluvinage et al., 2019). They can also secrete a wide range of cytokines including chemokines. Historically, microglia were often described as resting (i.e., ramified), but this phrasing failed to convey the dynamic remodeling of their fine processes and constitutive immunosurveillance activity, and are now termed homeostatic (Boche et al., 2013; Lawson et al., 1993). This morphology was in contrast to a more amoeboid phenotype microglia can also obtain, which was referred to as macrophages, but now is more commonly referred to as activated to avoid confusion with infiltrating cells (Arcuri et al., 2017). Both morphological and physiological properties have been used to identify microglial cells. The markers frequently used to identify microglia are CD68, MHC class II, CD11b or Iba1. However, since these markers are also expressed on other myeloid cells, they fail to distinguish between resident microglia and infiltrating macrophages.

The importance of microglia in most neurodegenerative diseases, such as multiple sclerosis and Alzheimer's disease, is increasingly appreciated (Pena-Altamira et al., 2016; Wang and Colonna, 2019). As microglia are highly plastic, the local disease environment, where microglia are in close interaction with other CNS cell types, differs between different pathologies and different regions leading to various phenotypes. Therefore, the microglial phenotype is disease-dependent, influenced by neighboring cell types and disease pathologies such as aggregated amyloid-beta (Bachiller et al., 2018). Neurodegenerative diseases such as multiple sclerosis are associated with infiltration of peripheral monocytes/macrophages that

65   contribute to disease pathogenesis (Meyer-Luehmann and Prinz, 2015). Many markers used

66   for the identification of microglia are also present in macrophages, as both cell types are

67   myeloid and share many transcriptional programs. Given a lack of reliable markers that can

68   distinguish between resident microglia and infiltrating myeloid cells, the specific function of

69   microglia in CNS diseases has been difficult to ascertain.

70   During the past few years, our group and others have generated bulk and single-cell

71   transcriptomics data to identify specific markers of human and mouse microglia (Bachiller et

72   al., 2018; Bennett et al., 2016; Butovsky et al., 2014; Chiu et al., 2013; Fahrenhold et al.,

73   2018; Gosselin et al., 2017; Hickman et al., 2013; Katsumoto et al., 2014; Konishi et al.,

74   2017; Marta Olah, 2019; Olah et al., 2018). Bennett *et al* identified Transmembrane protein

75   119 (TMEM119) as a specific marker of human and mouse microglia and generated an anti-

76   TMEM119 monoclonal antibody to detect microglia *in situ* (Bennett et al., 2016).

77   TMEM119, an evolutionarily conserved 58-kDa type 1 transmembrane protein, was

78   originally identified as a regulator of osteoblast differentiation. It is also expressed on human

79   osteoblasts and follicular dendritic cells. Mice homozygous for a targeted deletion of the

80   *Tmem119* gene exhibit growth retardation associated with delayed endochondral bone

81   ossification and impaired osteoblast differentiation(Hisa et al., 2011). Although the role of

82   TMEM119 in bone development is becoming clear, whether TMEM119 is involved in

83   microglia development and function is not known.

84   In an effort to develop a reliable tool for studying microglia, we have generated a novel

85   microglia reporter mouse strain where the tdTomato fluorescence gene was knocked-in

86   between the coding sequence of exon 2 and the termination codon in the 3' UTR of the

87   *Tmem119* gene thus preserving endogenous *Tmem119* expression. Using

88   immunofluorescence and flow cytometry analyses, we demonstrate that the TMEM119-

89   tdTomato signal is detected in the brain and spinal cord, is specific to microglia and is not

90   detected in peripheral myeloid cells. Using two-photon microscopy, we also show that our

91   *Tmem119-tdTomato* knock-in mouse strain is reliable for live imaging of microglia in naïve

92   mice as well as in mice that were exposed to brain injury.

93

94   **2. Materials and Methods**

95   **2.1. Mice**

96   *Tmem119-tdTomato* reporter mice were generated in BioCytogen Co, Ltd (Beijing, China).

97   Wild-type C57BL/6J mice were purchased from the Jackson Laboratory (Maine, USA) and

98   were crossed with the *Tmem119-tdTomato* mice. Animals were housed in the pathogen-free

99   animal facility at Columbia University Medical Center, in accordance with the guidelines of

100   the Committee of Animal Research at Columbia University and the National Institutes of

101   Health animal research guidelines as set forth in the Guide for the Care and Use of

102   Laboratory Animals. All studies were performed in compliance with procedures approved by

103   Columbia University Institutional Animal Care and Use Committee.

104   **2.2. Generation of the Tmem119-tdTomato knock-in mice using CRISPR/Cas9**

105   The Tmem119-tdTomato knock-in mouse strain was generated using CRISPR/Cas9

106   technology. Briefly, eight single-guide RNAs (sgRNA, see **supplementary File 1**) were

107   designed to target the sequence of the stop codon of murine *Tmem119* locus. The activity of

108   the CRISPR/Cas9 was assessed using a UCA kit. The results of genotyping with the UCA kit

109   showed that one sgRNA (sgRNA #4) was transcribed successfully with required

110   concentration (**supplementary File 1**). Following embryo microinjection using a

111   micromanipulator, embryos were cultured to the two-cell stage, followed by transfer into

112   pseudopregnant C57BL/6 females. The founders were genetically examined by amplifying

113   sequences spanning the 5' and 3' junction and including the entire inserted transgene. The

114   detailed workflow of the mouse line design, plasmid construction, Southern blot study

115   design, microinjection and founder genotyping is shown (**Supplementary File 1**).

116   **2.3. DNA isolation and genotyping**

117   Mouse genomic DNA was isolated from tail biopsies (0.5-1 cm) and following overnight

118   digestion at 55□ into 500 uL of buffer containing 100 mM Tris-HCl (pH 8.0), 5 mM EDTA

6

119   (pH 8.0), 200 mM NaCl, 0.2% SDS and 0.1 mg/mL Proteinase K. The samples were gently

120   mixed and cooled down at room temperature for 10-15 min. After centrifugation at 12000

121   rpm for 15 min, 400 uL of the supernatants were collected and gently mixed with the same

122   volume of isopropanol. After centrifugation at 12000 rpm for 10 min, the pellets were

123   washed by gently mixing with 700 uL of 75% ice-cold ethanol. After centrifugation at 12000

124   rpm for 5 min, the DNA pellets were harvested and air-dried at room temperature for 5 min.

125   The DNA was dissolved in 100 uL of distilled water at 55□ for two hours, and 100 ng DNA

126   were used for PCR reaction. Wild-type primers (562bp): Forward: 5'-

127   CAGAACCTCCGGTCTCCAGCTAGAG-3';   Reverse: 5'-

128   AGAGAAGTGGTGCGTTAGGGTGAAG-3'; Knock-in primers (299bp): Forward: 5'-

129   CCACCACCTGTTCCTGTACG-3';   Reverse: 5'-

130   AGAGAAGTGGTGCGTTAGGGTGAAG-3'. The PCR conditions were as follows: 1) 95□

131   for 15 min; 2) 35 cycles at 94□ for 45 sec, 60□ for 1 min, and 72□ for 1 min; 3) 72□ for 5

132   min. PCR products were separated on 2% Agarose gel. Detailed analysis of the genotyping

133   strategy is provided (**Supplementary File 2**).

134   **2.4. RNA isolation and real-time quantitative PCR**

135   Animals were humanely killed by CO_2 and transcardially perfused with ice-cold PBS. The

136   left-side half brains were harvested and frozen in dry ice and stored at -80C. RNA was

137   isolated using RNeasy Plus Micro Kit (#74034; QIAGEN, USA), and 10 uL of RNA was

138   reversely transcribed into cDNA using the High-Capacity cDNA Reverse Transcription Kit

139   (#4368814; Thermo Fisher Scientific, USA) following the manufacturer's instructions. The

140   *Tmem119* gene expression was detected by real-time quantitative PCR using TaqMan Fast

141   Advanced Master Mix (#4444557; Thermo Fisher Scientific) and *Tmem119* TaqMan Gene

142   Expression Assay (#Mm00525305_m1; Thermo Fisher Scientific). *Gapdh* TaqMan Gene

143   Expression Assay (#Mm99999915_g1; Thermo Fisher Scientific) was applied as an internal

144 amplification control. The PCR conditions were as follows: 50□ for 2 min, 95□ for 2 sec,

145 and followed by 40 cycles at 95□ for 1 sec and 60□ for 20 sec. The gene expression of

146 *Tmem119* relative to *Gadph* was quantified by the ΔΔCt method.

147 **2.5. Immunofluorescence staining**

148 Animals were humanely killed by CO_2 and and transcardially perfused with ice-cold PBS.

149 The right-side half brains were harvested and fixed in 4% paraformaldehyde (made in PBS;

150 #15710, Electron Microscopy Sciences, USA) at 4□ for 6 days. After dehydration in 30%

151 sucrose (made in PBS; #57-50-1, Affymetrix, USA), 30-μm thick free-floating sections were

152 sliced using the Cryostat CM3050S (Leica, Germany). For immunostaining, sections were

153 washed in PBS three times (10 min each), and incubated in blocking buffer (3% BSA

154 (#A7906, Sigma, USA) in PBS supplemented with 0.1% Triton X-100 (#9002-93-1; Sigma))

155 at room temperature for one hour. Primary antibodies (rabbit anti-TMEM119 (1:500;

156 #ab209064; Abcam, USA), mouse anti-TMEM119 (1:100; #853302, BioLegend, USA),

157 rabbit anti-Iba1 (1:500; #019-19741; Wako, Japan), mouse anti-NeuN (1:500; #MAB377,

158 Millipore, USA), rabbit anti-GFAP (1:500; #ZO334; Dako, USA), rabbit anti-Olig2 (1:500;

159 #AB9610; Millipore, USA) diluted in 1% BSA (in PBS) were further applied to the sections

160 at 4°C overnight. After being washed in PBS four times (10 min each), the sections were

161 incubated in species-matched secondary antibodies conjugated with 488 diluted in 1% BSA

162 (in PBS) at room temperature for one hour. Sections were washed again in PBS for four times

163 (10 min each), and mounted on slides with mounting media with DAPI (#NC9524612;

164 Vector Laboratories, USA), and imaged using confocal microscope (LSM700, Zeiss,

165 Germany).

166 **2.6. Flow cytometry**

167 Animals were humanely killed by CO_2 and blood was collected followed by perfusion with

168 ice-cold PBS. Brain, spinal cord, lung, heart, liver, spleen, kidney and intestine were

169   harvested, and homogenized in 2% FBS (in PBS). The cells were collected by centrifuging at

170   300g, 4□ for 10 min and were resuspended in MACS buffer (1% FBS in PBS supplemented

171   with 0.4% 0.5 M EDTA). The red blood cells were lysed by incubating with the same volume

172   of ACK lysis buffer (#A1049201, Gibco, USA). Cells were resuspended after being washed

173   twice in MACS buffer and analyzed by BD Accuri C6 flow cytometer (BD Biosciences,

174   USA). The blood samples were incubated with $10\times$ volume of RBC Lysis Solution

175   (#1045703, QIAGEN) at room temperature for 10 min. After being washed twice in MACS

176   buffer, the cells were resuspended and analyzed by BD Accuri C6. Microglia were isolated as

177   previously described (Butovsky et al., 2014; Olah et al., 2012; Verheijden et al., 2015).

178   Briefly, mice were humanely killed by CO2 and transcardially perfused with ice-cold PBS.

179   The brain tissues were quickly dissected and single cell suspensions were prepared and

180   separated using a 37%/70% Percoll gradient (#GE17-0891-01, GE Healthcare). Myelin was

181   removed from the top layer and mononuclear cells were isolated from the interface. The cells

182   were incubated with mouse anti-CD45-FITC (1:200; #103108, BioLegend) and mouse anti-

183   CD11b-APC (1:80; #101212, BioLegend) for 30 minutes on ice in the dark. Cell suspensions

184   were analyzed using the BD FACS Canto (BD Biosciences), and data were analyzed with

185   FlowJo software (TreeStar, USA).

186   **2.7. Two-photon laser injury inside the cortex**

187   A highly localized injury was achieved by focusing a two-photon laser beam (□1 μm in

188   size) in the superficial layer of the cortex through the open skull window. The wavelength

189   of the two-photon laser was set at 800 nm and the laser power was □60–80 mW at the

190   sample. The beam was parked at the desired position for approximately 3-5 seconds to

191   create a small injury site as indicated by a bright autofluorescent sphere (□30 μm in

192   diameter) around the focal point of the beam. The injury was confined to the area □25–35

9

193   μm in diameter around the laser focal point, because microglia within this area lost their

194   tdtomato immediately after laser ablation, whereas those ☐50 μm from the injury site still

195   responded to the ablation. The laser-induced focal ablation is a useful injury model, as the

196   site and degree of injury are easy to control, and the response of microglia toward the

197   injury is highly reproducible.

198   **2.8. *In vivo* imaging of microglia with two-photon microscopy**

199   To investigate microglia in vivo in intact brain, tdTomato-labeled microglia were imaged

200   by two-photon microscopy through a small craniotomy. Briefly, 2-3 month-old *Tmem119-*

201   *tdTomato* mice were anesthetized intraperitoneally with ketamine (200 mg/kg body

202   weight) and xylazine (30 mg/kg body weight) in 0.9% NaCl solution. A region (☐1 mm in

203   diameter) over primary sensory cortex was first thinned with a high-speed drill under a

204   dissecting microscope and then opened either with a needle or forceps. A drop (☐200 μl)

205   of artificial mouse cerebrospinal fluid (ACSF) was applied on the exposed region for the

206   duration of the experiment. The skull surrounding the open window was attached to a

207   custom-made steel plate to reduce respiratory-induced movement. The animal was placed

208   under a two-photon microscope (Scientifica Hyperscope, East Sussex, UK) while still

209   under anesthesia and temperature maintained with a heating pad (~37°C). The two-photon

210   laser was tuned to the excitation wavelength for tdTomato (1000 nm). All experiments

211   were performed using a 1.1–numerical aperture (NA) 25× objective lens immersed in

212   ACSF to obtain 62.5X high-magnification (166.4 μm × 166.4 μm; 512 × 512 pixels; 1.5-

213   μm step) images for neuronal analysis. The maximum imaging depth was ☐120 μm from

214   the pial surface. Images were acquired using low laser power (< 30 mW at the sample) and

215   a low-pass emission filter (<700 nm).

216   **2.9. Image processing and quantification**

10

217   All image processing and quantification were performed with Image J software (NIH). All

218   z-stacks of images were projected along the z-axis to recreate a two-dimensional

219   representation of 3D structures. To quantify the microglia response to laser induced injury,

220   we measured the number of microglia processes entering from outer area Y into inner area

221   as a function of time. The number of red pixels in area X or Y were measured at each time

222   point ($R_x(t)$ or $R_y(t)$, and the microglial response was defined as $R(t) = [R_x(t) -$

223    $R_x(0)]$(Bennett et al., 2016)$/R_y(0)$. To account for signal intensity differences among

224   different experiments, we thresholded every image so that all processes had the maximum

225   value (255), and all background was set to 0. We then counted the number of white pixels

226   in area X over time ($Rx(t)$) and compared it with the first picture taken immediately after

227   the ablation ($R_x(0)$). The number of white pixels corresponds to the region covered by

228   processes within the area X, and its increase over time provides a measure of the

229   microglial response. To account for the variability in the number of microglia located in

230   the outer area Y in different experiments, we calculated the microglial response relative to

231   the number of processes in the outer area Y immediately after the ablation ($R_y(0)$). The

232   microglial response at any time point ($R(t)$) is therefore given by $R(t) = (R_x(t) -$

233    $Rx(0))/R_y(0)$.

234   **2.10. Data analysis**

235   All data are presented as mean ± s.e.m., and were analyzed by GraphPad Prism 8. Unpaired

236   Student *t*-test and one-way ANOVA were used for group comparisons. $P < 0.05$ was

237   considered statistically significant.

11

238 **3. Results**

239 **3.1. Generation and validation of *Tmem119-tdTomato* reporter mice**

240 Here, we took advantage of the recent identification of TMEM119 as a specific marker of

241 human and murine microglia (Bennett et al., 2016) to generate a new tool for studying the

242 behavior and function of microglia in health and disease. We describe the generation and the

243 characterization of the *Tmem119-tdTomato* knock-in mouse strain where endogenous

244 *Tmem119* expression is preserved. A CRISPR/Cas9 strategy was used to insert tdTomato,

245 preceded by ribosome-skipping peptide porcine teschovirus-1 polyprotein (P2A), upstream of

246 the stop codon of murine *Tmem119*. Two founder lines were established for *Tmem119-*

247 *tdTomato* that were bred with wild-type mice on the C57BL/6 background to generate an on-

248 target sequence (**Figure 1A**). The data demonstrating the specific insertion of the transgene

249 into the *Tmem119* locus are shown (**Supplementary File 1**). Confirmation of the mouse

250 genotypes comparing WT mice to heterozygous or homozygous lines are shown (**Figure 1B**

251 and **Supplementary File 2**). To validate that the transgene insert does not affect endogenous

252 Tmem119 expression, we measured *Tmem119* gene expression by quantitative PCR. As

253 expected, we found no difference in *Tmem119* mRNA levels in brain homogenates by

254 comparing *Tmem119*$^{tdT/+}$ mice with wild-type controls (p = 0.9996; Student's *t*-test; **Figure**

255 **1C**). Next, to confirm that tdTomato is co-expressed with TMEM119, we used two

256 commercially available anti-TMEM119 antibodies (anti-intracellular and anti-extracellular

257 domain of TMEM119) to track the TMEM119 expression in coronal brain sections from 10

258 months old *Tmem119*$^{tdTomato/+}$ mice. Our data showed that both of the antibodies recognized

259 the tdTomato$^+$ cells, indicating that tdTomato$^+$ cells readily express TMEM119.

260

261 **3.2. TMEM119-tdTomato is expressed in CNS but not in peripheral tissues and blood**

12

262   To examine whether tdTomato is predominately expressed in the CNS of *Tmem119-*

263   *tdTomato* mice, we analyzed CNS and peripheral tissues and organs by immunofluorescence

264   and flow cytometry. Thus, we collected brain, spinal cord, blood, heart, kidney, lung,

265   intestine, spleen and liver from 3-month old *Tmem119*$^{tdTomato/+}$ mice. Immunofluorescence

266   staining showed that tdTomato positive cells were detected throughout the CNS regions,

267   including the olfactory bulb, the prefrontal cortex, the hippocampus, the thalamus, the

268   midbrain, the cerebellum and the spinal cord **(Figure 2A-I)**. In contrast, no tdTomato

269   expression was observed in peripheral tissues such as the heart, the kidney, the lung, the

270   intestine, the spleen and the liver (**Figure 2J-O**). To confirm these findings, we harvested cell

271   suspensions from these tissues as well as blood and measured the tdTomato expression by

272   flow cytometry. Based on a gating strategy the excludes doublets and debris (**Figure 2P**), we

273   detected 15.1% of events as tdTomato positive in the brains of *Tmem119*$^{tdTomato/+}$ mice, but

274   not in the brains of WT mice (**Figure 2Q**). Consistent with the histological analysis, there

275   was no tdTomato positive cells detected in peripheral tissues (**Figure 2S-X**) or blood (**Figure**

276   **2R**).

277

278   **3.3. TMEM119-tdTomato is constantly expressed in adult and aged CNS**

279   We have provided evidence to prove spatial expression of TMEM119-tdTomato that is

280   specific to the CNS. We further asked if TMEM119 expression is maintained in aged brains.

281   To address this question, we analyzed tdTomato expression in coronal brain sections from

282   different ages [Postnatal day (P)90, P300 and P540] of *Tmem119*$^{tdTomato/+}$ mice by

283   immunofluorescence staining. Our data show that TMEM119-tdTomato expression is

284   expressed in the brain of both young adult and aged mice (**Figure 3A-C**).

285

286   **3.4. TMEM119-tdTomato is expressed in Iba1^{+} cells but not in other CNS-resident cells**

13

287   Given that tdTomato is specifically expressed in microglia, we sought to examine whether

288   TMEM119 is microglial-specific or is also detectable in other CNS-resident cells such as

289   neurons, astrocytes and oligodendrocytes. To do this, we stained coronal brain sections of

290   *Tmem119*^{tdTomato/+} mice with a marker of each of these three cell types in addition to a

291   microglial marker. Thus, the following antibodies – against NeuN, GFAP, Olig2 and Iba1 -

292   were tested in the coronal brain sections from of *Tmem119*^{tdTomato/+} mice to detect neurons,

293   astrocytes, oligodendrocytes and microglia, respectively. Our data showed that tdTomato

294   expression was only detected in Iba1$^+$ cells but not in NeuN$^+$, GFAP$^+$ and Olig2$^+$ cells in the

295   brain (**Figure 4A-D**). These findings confirm that TMEM119 is exclusively expressed in

296   microglial cells in the brain.

297

298   **3.5. TMEM119-tdTomato is specifically expressed in microglia but not in infiltrating**

299   **immune cells in adult brain**

300   To further confirm that TMEM119-tdTomato$^+$ cells are indeed microglia, we used a Percoll

301   density gradient technique to isolate microglia from the brain of adult WT and

302   *Tmem119*^{tdTomato/+} mice. We then compared the tdTomato$^+$ cells to the CD45^{lo}CD11b$^+$

303   microglia. Based on the gating strategy showed in a representative experiment in **Figure 5A-**

304   **D**, we found 97.8% of live cells were CD45$^+$ in WT mice (**Figure 5E**) relative to 99.4% in

305   *Tmem119*^{tdTomato/+} mice (**Figure 5F**). Within the CD45$^+$ cells, 90.6% of this population was

306   tdTomato-positive in the *Tmem119*^{tdTomato/+} mice (**Figure 5H**), while no tdTomato was

307   detected in WT mice (**Figure 5G**). The tdTomato$^+$ cells from *Tmem119*^{tdTomato/+} mice were

308   further analyzed, and we found that they are all CD45^{lo}CD11b$^+$ microglia (**Figure 5I**). In the

309   reverse experiment, we found that 97.5% of CD45$^+$ cells in WT (**Figure 5J**) and 94.6% of

310   these cells in *Tmem119*^{tdTomato/+} mice (**Figure 5K**) are CD45^{lo}CD11b$^+$ microglia, and 96.6%

311   of the CD45^{lo}CD11b$^+$ microglia are tdTomato positive in *Tmem119*^{tdTomato/+} mice while none

14

312   are positive in WT mice (**Figure 5L**). Overall, our data demonstrate that all tdTomato$^+$ cells

313   are CD45^{lo}CD11b$^+$ microglia.

314

315   **3.6. Two-photon live imaging of TMEM119-tdTomato$^+$ microglia *in vivo* in a laser-**

316   **induced injury model**

317   To validate the *Tmem119-tdTomato* reporter mice as a useful tool to monitor the activity of

318   microglia *in vivo*, we elected to use a model of laser-induced injury to monitor microglia

319   response in the intact living brain. Using transcranial two-photon microscopy, we were able

320   to image the behavior of tdTomato-expressing parenchymal microglia through the open skull

321   window of anesthetized *Tmem119*$^{tdTomato/+}$ mice. Thus we performed a small laser ablation,

322   ~30 μm in diameter, inside the primary sensory cortex (**Figure 6A**). Time-lapse images (up

323   to150 minutes) show that microglia formed a spherical containment around the laser lesion

324   site. Within minutes after laser injury, the number of microglia entering from outer area (Y)

325   into inner area (X) is measured as a function of time showing rapid response of microglia to

326   the injury site (**Figure 6B, C**). During this period, the same cells also retracted those

327   processes that previously lay in directions opposite to the site of injury. Most of the cellular

328   content of each of the immediate neighbors was directed towards the damaged site within the

329   first 1-3 h (**Figure 6D, Supplementary Video 1**). Length changes of four processes marked

330   in **Figure 6D** were quantified as function of time (**Figure 6E**). These results indicate that the

331   *Tmem119-tdTomato* mouse strain is a viable model to monitor and analyze the activity and

332   the formation of microglia processes in neuroinflammatory disease models.

15

333 **4. Discussion**

334 Microglia are becoming the center of attention in the field of neurodegeneration and several

335 clinical trials are currently designed to manipulate microglial function in the context of

336 neurodegenerative diseases (Fu et al., 2019; Mullard, 2018; Subramaniam and Federoff,

337 2017). However, cultured microglia quickly lose their unique microglia signature once out of

338 the CNS, making the ability to study these cells difficult. Here, we present a model which

339 allows us to study microglial behavior *in vivo*, even in the presence of other innate immune

340 cells. Given the lack of markers that discriminate between microglia and infiltrated myeloid

341 cells that are shown to invade the CNS in neurodegenerative diseases, developing new tools

342 to detect and isolate microglia is becoming of high interest to the research community. In the

343 present study, we report a microglia-specific mouse strain that express the recently identified

344 microglia-specific marker Tmem119 (Bennett et al., 2016; Satoh et al., 2016). A knock-in

345 strategy was used to generate the *Tmem119-tdTomato* where *tdTomato* is placed between

346 exon 2 and the 3'UTR of *Tmem119* gene thus allowing the detection of TMEM119-positive

347 cells without affecting TMEM119 endogenous expression as shown by comparing Tmem119

348 expression in the brains of *Tmem119-tdTomato* and wild-type mice. The choice of tdTomato

349 as a reporter protein is because it provides a very bright red fluorescence (~3 fold higher than

350 EGFP)(Shaner et al., 2005) that is ideal for live imaging and potentially for generating double

351 reporter mice with GFP mice for studying microglia in relation to other GFP-labeled cell

352 types.

353 Using immunofluorescence and flow cytometry analysis we provide evidence that tdTomato

354 selectively labels microglial cells in the CNS but not peripheral myeloid cells. Satoh *et al*.

355 showed that TMEM119 could discriminate brain-residing microglial cells from circulating

356 macrophages, as this protein is expressed exclusively on ramified and amoeboid microglial

357 cells in the brain (Satoh et al., 2016). Additionally, we validate the specificity of two

16

358   commercially available anti-TMEM119 antibodies available at Abcam and Biolegend that

359   stain the intracellular and extracellular domains of TMEM119, respectively. In adult

360   Tmem119-tdTomato reporter mice, we found that TMEM119 is expressed throughout the

361   brain and the spinal cord. Strikingly, we did not detect the tdTomato signal in peripheral

362   lymphoid organs and the blood. Bennett and colleagues generated monoclonal antibodies to

363   the intracellular and extracellular domains of TMEM119 that enable the immunolabeling of

364   microglia in histological sections as well as isolation of microglia by FACS (Bennett et al.,

365   2016). The study by Bennett *et al.* showed that Tmem119 immunoreactivity is developmentally

366   regulated as Tmem119 expression did not appear until postnatal day 3 and 6 (Bennett et al.,

367   2016). These findings are in agreement with the present study where we did not detect

368   tdTomato expression in the brain of newborn mice (data not shown).

369   During the past few years and with the availability of instrumental gene profiling techniques

370   that can process very small numbers of cells, mainly from human autopsies and biopsies, led

371   to a series of reports generating transcriptomics profiling of human and murine microglia at

372   the bulk and the single-cell levels (Butovsky et al., 2014; Chiu et al., 2013; Hickman et al.,

373   2013; Marta Olah, 2019; Masuda et al., 2019; Olah et al., 2018; Zhang et al., 2014). Several

374   microglia clusters have been identified with specific gene signatures that are associated with

375   homeostatic and active microglia. In our recent study examining the gene signature of the

376   aged human brain using fresh brain autopsies from aged subjects, we found that *Tmem119*

377   gene expression is found in microglia purified from aged human brain (Olah et al., 2018).

378   This is consistent with our present data in the *Tmem119-tdTomato* mice where TMEM119

379   expression is readily present in aged microglia (1.6 years old mice) at the protein level.

380   More recently, given the heterogeneous nature of the human brain, we have utilized a

381   single cell RNA-seq approach to analyze microglia heterogeneity across several

382   neurological disorders including Alzheimer's disease, Parkinson's disease and epilepsy.

17

383   Computational analysis identified nine distinct microglia subsets that express different

384   levels of *Tmem119* (Marta Olah, 2019*)*. In our *Tmem119-tdTomato* mice, although

385   TMEM119 expression was detected throughout the healthy adult and aged brains, it

386   remains possible that TMEM119 expression will be regulated in a disease state where

387   microglia are subject to neuroinflammatory stimuli. Another recent study reporting single-

388   cell RNA-seq analyses of microglia in mice and humans showed that Tmem119 is among

389   the most highly differentially regulated genes during development as it is highly expressed

390   in postnatal microglia. The authors found that Tmem119 is expressed in homeostatic

391   microglia clusters in healthy brains whereas microglia clusters that are associated with

392   multiple sclerosis and are characterized as activated clusters express lower levels of

393   Tmem119 (Masuda et al., 2019). Single-cell RNA-seq approaches are an instrumental

394   approach to define heterogeneous cell subsets. Crossing the Tmem119-tdTomato mice

395   with mouse models of neurodegenerative diseases such as Alzheimer's or Parkinson's

396   disease will provide valuable information about the different subsets of TMEM119-

397   positive microglia in a disease state.

398   In addition to the goals discussed above that lead to the generation of microglia-specific

399   reporter mice based on the TMEM119 approach, we were interested in having in hand a

400   reporter model where we can image microglia *in vivo* in live animals. Our two-photon

401   imaging data demonstrate that the *Tmem119-tdTomato* mice are an excellent model for live

402   observation of microglia to analyze their response to any type of stimulation or stress as

403   reported using laser-induced injury. Indeed, our two-photon analysis reported the number of

404   tdTomato-positive microglia processes entering the site of injury, processes formation and

405   their retraction vis-à-vis the site of injury. Our findings suggest that the *Tmem119-tdTomato*

406   mouse strain is an excellent model for imaging and analyzing microglia activity alone or in

407   relation to other CNS-resident or infiltrated immune cells in disease models such as multiple

408   sclerosis, Parkinson's disease and Alzheimer's disease.

409   In conclusion, our study provides a microglia-specific reporter mouse model based on

410   the Tmem119 microglia marker. This *Tmem119-tdTomato* mouse strain will be a critical tool

411   for microglia-focused research in health and disease. Additionally, crossing this mouse strain

412   with other reporter mice expressing other fluorescent proteins specific for CNS-resident cells

413   and peripheral immune cells will provide unique mouse models to study the interaction

414   between microglia and other CNS resident or infiltrated cells.

415

416

417

418

419

420 **Conflicts of interest**

421 Samuel Hasson was employed by Pfizer and is a current employee of Amgen.

422

423 **Acknowledgments**

427

428 **References**

429 Arcuri, C., Mecca, C., Bianchi, R., Giambanco, I., Donato, R., 2017. The Pathophysiological
430 Role of Microglia in Dynamic Surveillance, Phagocytosis and Structural Remodeling of the
431 Developing CNS. Front Mol Neurosci 10, 191.
432 Bachiller, S., Jimenez-Ferrer, I., Paulus, A., Yang, Y., Swanberg, M., Deierborg, T., Boza-
433 Serrano, A., 2018. Microglia in Neurological Diseases: A Road Map to Brain-Disease
434 Dependent-Inflammatory Response. Front Cell Neurosci 12, 488.
435 Bennett, M.L., Bennett, F.C., Liddelow, S.A., Ajami, B., Zamanian, J.L., Fernhoff, N.B.,
436 Mulinyawe, S.B., Bohlen, C.J., Adil, A., Tucker, A., Weissman, I.L., Chang, E.F., Li, G.,
437 Grant, G.A., Hayden Gephart, M.G., Barres, B.A., 2016. New tools for studying microglia in
438 the mouse and human CNS. Proc Natl Acad Sci U S A 113, E1738-1746.
439 Boche, D., Perry, V.H., Nicoll, J.A., 2013. Review: activation patterns of microglia and their
440 identification in the human brain. Neuropathol Appl Neurobiol 39, 3-18.
441 Butovsky, O., Jedrychowski, M.P., Moore, C.S., Cialic, R., Lanser, A.J., Gabriely, G.,
442 Koeglsperger, T., Dake, B., Wu, P.M., Doykan, C.E., Fanek, Z., Liu, L., Chen, Z., Rothstein,
443 J.D., Ransohoff, R.M., Gygi, S.P., Antel, J.P., Weiner, H.L., 2014. Identification of a unique
444 TGF-beta-dependent molecular and functional signature in microglia. Nat Neurosci 17, 131-
445 143.
446 Chiu, I.M., Morimoto, E.T., Goodarzi, H., Liao, J.T., O'Keeffe, S., Phatnani, H.P., Muratet,
447 M., Carroll, M.C., Levy, S., Tavazoie, S., Myers, R.M., Maniatis, T., 2013. A
448 neurodegeneration-specific gene-expression signature of acutely isolated microglia from an
449 amyotrophic lateral sclerosis mouse model. Cell Rep 4, 385-401.
450 Colonna, M., Butovsky, O., 2017. Microglia Function in the Central Nervous System During
451 Health and Neurodegeneration. Annu Rev Immunol 35, 441-468.
452 Fahrenhold, M., Rakic, S., Classey, J., Brayne, C., Ince, P.G., Nicoll, J.A.R., Boche, D., Mrc,
453 C., 2018. TREM2 expression in the human brain: a marker of monocyte recruitment? Brain
454 Pathol 28, 595-602.
455 Fu, W.Y., Wang, X., Ip, N.Y., 2019. Targeting Neuroinflammation as a Therapeutic Strategy
456 for Alzheimer's Disease: Mechanisms, Drug Candidates, and New Opportunities. ACS Chem
457 Neurosci 10, 872-879.
458 Gosselin, D., Skola, D., Coufal, N.G., Holtman, I.R., Schlachetzki, J.C.M., Sajti, E., Jaeger,
459 B.N., O'Connor, C., Fitzpatrick, C., Pasillas, M.P., Pena, M., Adair, A., Gonda, D.D., Levy,
460 M.L., Ransohoff, R.M., Gage, F.H., Glass, C.K., 2017. An environment-dependent
461 transcriptional network specifies human microglia identity. Science 356.
462 Graeber, M.B., Streit, W.J., 1990. Microglia: immune network in the CNS. Brain Pathol 1, 2-
463 5.
464 Hanisch, U.K., Kettenmann, H., 2007. Microglia: active sensor and versatile effector cells in
465 the normal and pathologic brain. Nat Neurosci 10, 1387-1394.
466 Hickman, S.E., Kingery, N.D., Ohsumi, T.K., Borowsky, M.L., Wang, L.C., Means, T.K., El
467 Khoury, J., 2013. The microglial sensome revealed by direct RNA sequencing. Nat Neurosci
468 16, 1896-1905.
469 Hisa, I., Inoue, Y., Hendy, G.N., Canaff, L., Kitazawa, R., Kitazawa, S., Komori, T.,
470 Sugimoto, T., Seino, S., Kaji, H., 2011. Parathyroid hormone-responsive Smad3-related
471 factor, Tmem119, promotes osteoblast differentiation and interacts with the bone
472 morphogenetic protein-Runx2 pathway. J Biol Chem 286, 9787-9796.
473 Katsumoto, A., Lu, H., Miranda, A.S., Ransohoff, R.M., 2014. Ontogeny and functions of
474 central nervous system macrophages. J Immunol 193, 2615-2621.
475 Konishi, H., Kobayashi, M., Kunisawa, T., Imai, K., Sayo, A., Malissen, B., Crocker, P.R.,
476 Sato, K., Kiyama, H., 2017. Siglec-H is a microglia-specific marker that discriminates

477   microglia from CNS-associated macrophages and CNS-infiltrating monocytes. Glia 65, 1927-
478   1943.

479   Lawson, L.J., Matyszak, M.K., Perry, V.H., 1993. Lessons from microglia in special sites.
480   Clin Neuropathol 12, 310-313.

481   Marta Olah, V.M., Naomi Habib, Mariko Taga, Christina Yung, Maria Cimpean, Anthony
482   Khairalla, Danielle Dionne, Sarah Hopp, Matthew P. Frosch, Bradley T. Hyman, Thomas
483   Beach, Rani Sarkis, Garth R Cosgrove, Jeffrey Helgager, Jeffrey A. Golden, Page B. Pennell,
484   Julie A. Schneider, David A. Bennett, Aviv Regev, Wassim Elyaman, Elizabeth M.
485   Bradshaw, Philip L. De Jager, 2019. A single cell-based atlas of human microglial states
486   reveals associations with neurological disorders and histopathological features of the aging
487   brain. BioRxiv.org.

488   Masuda, T., Sankowski, R., Staszewski, O., Bottcher, C., Amann, L., Sagar, Scheiwe, C.,
489   Nessler, S., Kunz, P., van Loo, G., Coenen, V.A., Reinacher, P.C., Michel, A., Sure, U.,
490   Gold, R., Grun, D., Priller, J., Stadelmann, C., Prinz, M., 2019. Spatial and temporal
491   heterogeneity of mouse and human microglia at single-cell resolution. Nature 566, 388-392.

492   Meyer-Luehmann, M., Prinz, M., 2015. Myeloid cells in Alzheimer's disease: culprits,
493   victims or innocent bystanders? Trends Neurosci 38, 659-668.

494   Mullard, A., 2018. Microglia-targeted candidates push the Alzheimer drug envelope. Nat Rev
495   Drug Discov 17, 303-305.

496   Olah, M., Amor, S., Brouwer, N., Vinet, J., Eggen, B., Biber, K., Boddeke, H.W., 2012.
497   Identification of a microglia phenotype supportive of remyelination. Glia 60, 306-321.

498   Olah, M., Patrick, E., Villani, A.-C., Xu, J., White, C.C., Ryan, K.J., Piehowski, P., Kapasi,
499   A., Nejad, P., Cimpean, M., Connor, S., Yung, C.J., Frangieh, M., McHenry, A., Elyaman,
500   W., Petyuk, V., Schneider, J.A., Bennett, D.A., De Jager, P.L., Bradshaw, E.M., 2018. A
501   transcriptomic atlas of aged human microglia. Nat Commun 9, 539.

502   Pena-Altamira, E., Prati, F., Massenzio, F., Virgili, M., Contestabile, A., Bolognesi, M.L.,
503   Monti, B., 2016. Changing paradigm to target microglia in neurodegenerative diseases: from
504   anti-inflammatory strategy to active immunomodulation. Expert Opin Ther Targets 20, 627-
505   640.

506   Pluvinage, J.V., Haney, M.S., Smith, B.A.H., Sun, J., Iram, T., Bonanno, L., Li, L., Lee,
507   D.P., Morgens, D.W., Yang, A.C., Shuken, S.R., Gate, D., Scott, M., Khatri, P., Luo, J.,
508   Bertozzi, C.R., Bassik, M.C., Wyss-Coray, T., 2019. CD22 blockade restores homeostatic
509   microglial phagocytosis in ageing brains. Nature 568, 187-192.

510   Satoh, J., Kino, Y., Asahina, N., Takitani, M., Miyoshi, J., Ishida, T., Saito, Y., 2016.
511   TMEM119 marks a subset of microglia in the human brain. Neuropathology 36, 39-49.

512   Shaner, N.C., Steinbach, P.A., Tsien, R.Y., 2005. A guide to choosing fluorescent proteins.
513   Nat Methods 2, 905-909.

514   Subramaniam, S.R., Federoff, H.J., 2017. Targeting Microglial Activation States as a
515   Therapeutic Avenue in Parkinson's Disease. Front Aging Neurosci 9, 176.

516   Verheijden, S., Beckers, L., Casazza, A., Butovsky, O., Mazzone, M., Baes, M., 2015.
517   Identification of a chronic non-neurodegenerative microglia activation state in a mouse model
518   of peroxisomal β-oxidation deficiency. Glia 63, 1606-1620.

519   Wang, S., Colonna, M., 2019. Microglia in Alzheimer's disease: A target for immunotherapy.
520   J Leukoc Biol.

521   Wu, Y., Dissing-Olesen, L., MacVicar, B.A., Stevens, B., 2015. Microglia: Dynamic
522   Mediators of Synapse Development and Plasticity. Trends Immunol 36, 605-613.

523   Zhang, Y., Chen, K., Sloan, S.A., Bennett, M.L., Scholze, A.R., O'Keeffe, S., Phatnani, H.P.,
524   Guarnieri, P., Caneda, C., Ruderisch, N., Deng, S., Liddelow, S.A., Zhang, C., Daneman, R.,
525   Maniatis, T., Barres, B.A., Wu, J.Q., 2014. An RNA-sequencing transcriptome and splicing

526   database of glia, neurons, and vascular cells of the cerebral cortex. J Neurosci 34, 11929-
527   11947.
528

529 **Figure Legends**

530 **Figure 1. Generation and validation of *Tmem119-tdTomato* reporter mice**. (**A**) Schematic

531 of engineering strategy to create the *Tmem119-tdTomato* reporter mice. A DNA sequence of

532 GSG-3xFlag-P2A-tdTomato was inserted between the exon 2 and 3'UTR in the *Tmem119*

533 gene by CRISPR/Cas9 technology. E, exon; UTR, untranslated region. (**B**) A representative

534 genotyping result showing the genotype of WT (with a 562-bp size band), *Tmem119*$^{\text{tdTomato/+}}$

535 (with a 562-bp and 299-bp size band) and *Tmem119*$^{\text{tdTomato/tdTomato}}$ (with a 299-bp band). tdT,

536 tdTomato. (**C**) The gene expression of *Tmem119* relative to *Gapdh* in central nervous system

537 was detected between 3-month old WT and *Tmem119*$^{\text{tdTomato/+}}$ mice ($n = 3$ each). Data are

538 presented in mean ± s.e.m. (**D**) TMEM119 (green) was stained in coronal brain sections from

539 10-month old *Tmem119*$^{\text{tdTomato/+}}$ mice by an intracellular (left; clone 28-3, Abcam) and an

540 extracellular (right; clone A16075D, BioLegend) antibodies. Red, tdTomato. Yellow arrows,

541 colocalized staining. White arrows, uncolocalized staining. Scale bar, 50 μm.

542

543 **Figure 2. TdTomato is expressed in the adult CNS but not in the blood nor in**

544 **peripheral tissues.** A representative image of sagittal section in brain (**A**) and coronal

545 section in spinal cord (H) from 3-month old *Tmem119*$^{\text{tdTomato/+}}$ mice. Sections: 16-μm thick.

546 Scale bar, 500 μm. TdTomato (red) were detected in cells through over different regions of

547 central nervous system, such as olfactory bulb (**B**), prefrontal cortex (**C**), hippocampus (**D**),

548 thalamus (**E**), midbrain (**F**), cerebellum (**G**) and spinal cord (**I**). Sections were mounted in

549 media with DAPI (blue). Scale bar, 50 μm. TdTomato were not detected in cells in peripheral

550 tissues such as heart (**J**), kidney (**K**), lung (**L**), intestine (**M**), spleen (**N**) and liver (**O**).

551 Sections, 16-μm thick. Scale bar, 50 μm. TdTomato were measured in CNS, blood and

552 peripheral tissues from 3-month old *Tmem119*$^{\text{tdTomato/+}}$ mice by flow cytometry, and tdTomato

553 positive cells were only detected in CNS tissues (**Q**) but not in blood (**R**) and peripheral

24

554   tissues such as heart (**S**), kidney (**T**), lung (**U**), intestine (**V**), spleen (**W**) and liver (**X**), based

555   on a gating strategy (**P**). SSC-A, side scatter (area); FSC-A, forward scatter (area); SSC-H,

556   side scatter (hight); FSC-H, forward scatter (hight); CNS, central nervous system; WT, wild

557   type; tdT, tdTomato.

558

559   **Figure 3. TdTomato is consistently expressed in the adult and aged CNS.** TdTomato$^+$

560   cells (red) were detectable in the coronal brain sections from postnatal 90 days (**A**), 300 days

561   (**B**) and 540 days (**C**). **a**, **b**, and **c**, are amplified images from each staining. P, postnatal; VI,

562   the fourth layer of neocortex; CA1, the first region of hippocampal circuit. Sections, 30-µm

563   thick. Scale bar, 100 µm.

564

565   **Figure 4. TdTomato is specifically expressed in Iba1$^+$ microglia/macrophages but not in**

566   **other CNS-resident cells**. TdTomato$^+$ cells (red) were colocalized with

567   microglia/macrophage marker Iba1$^+$ cells (**A**, green), but not neuronal marker NeuN$^+$ (**B**,

568   green), astrocyte marker GFAP$^+$ (**C**, green) or oligodendrocyte marker Olig2$^+$ (**D**, green) cells

569   in the coronal brain sections of adult *Tmem119*$^{\text{tdTomato/+}}$ mice by immunofluorescence staining.

570   (*n* = 3 sections per mouse, *N* = 3 mice). Red, tdTomato. Blue, DAPI. **a**, **b**, **c**, and **d**, are

571   amplified images from each staining. VI, the fourth layer of neocortex; CA1, the first region

572   of hippocampal circuit. Arrowheads, colocalized staining. Sections, 30-µm thick. Scale bar,

573   100 µm.

574

575   **Figure 5. TdTomato is specifically expressed in microglia but not in infiltrating immune**

576   **cells in the adult brain.** (**A-D**) Flow cytometry analysis to gate out cells of interest (**A**),

577   single cells (**B, C**) and live cells (**D**). (**E-I**) tdTomato$^+$ cells in the brain tissues of WT (**G**) vs

578   *Tmem119*$^{\text{tdTomato/+}}$ (**H**) mice are gated based on the CD45$^+$ cells in WT (**E**) or

25

579     $Tmem119^{tdTomato/+}$ (**F**) mice. CD45^{lo}CD11b$^+$ cells (**I**) were further gated out of tdTomato$^+$ cells

580   (**H**) in $Tmem119^{tdTomato/+}$ mice. (**E, F, J-L**) CD45^{lo}CD11b$^+$ cells (**J, K**) were gated out of

581   CD45$^+$ cells in WT (**E**) or $Tmem119^{tdTomato/+}$ (**F**) mice, and the tdTomato$^+$ cells in WT vs

582     $Tmem119^{tdTomato/+}$ mice (**L**) were further gated based on the CD45^{lo}CD11b$^+$ cells (**J, K**). SSC-

583   A, side scatter (area); SSC-H, side scatter (hight); SSC-W, side scatter (width); FSC-A,

584   forward scatter (area); FSC-H, forward scatter (hight); FSC-W, forward scatter (width); WT,

585   wild type; tdT, tdTomato; CD45^{lo}, low expression of CD45. The number beside or within the

586   gate indicates percentage of cells in each plot.

587

588   **Figure 6**. **Two-photon live imaging of tdTomato$^+$ microglia *in vivo* after laser-mediated**

589   **injury**. (**A**) After a localized ablation inside the primary sensory cortex, neighboring

590   Tmem119-tdTonmato$^+$ microglia respond quickly with extended processes and bulbous

591   termini. Time-lapse images show that microglia formed a spherical containment around the

592   laser lesion site. Scale bar, 30 µm. (**B**) To quantify the laser injury-induced microglial

593   response, the number of microglia processes entering from outer area Y into inner area X is

594   measured as a function of time. The number of red pixels in area X or Y were measured at

595   each time point ($R_x(t)$ or $R_y(t)$, and the microglial response was defined as $R(t) = [R_x(t) -$

596     $R_x(0)]/R_y(0)$. Scale bar, 30 µm. (**C**) Microglia response over 1 hour after laser injury. (**D**) The

597   same cell extends its processes towards the laser lesion site (marked by yellow x), and

598   retracts the ones in the opposite direction to the injured site. Scale bar, 10 µm. (**E**) Length

599   changes of four processes marked in **D** as a function of time. Scale bar, 10 µm.

600

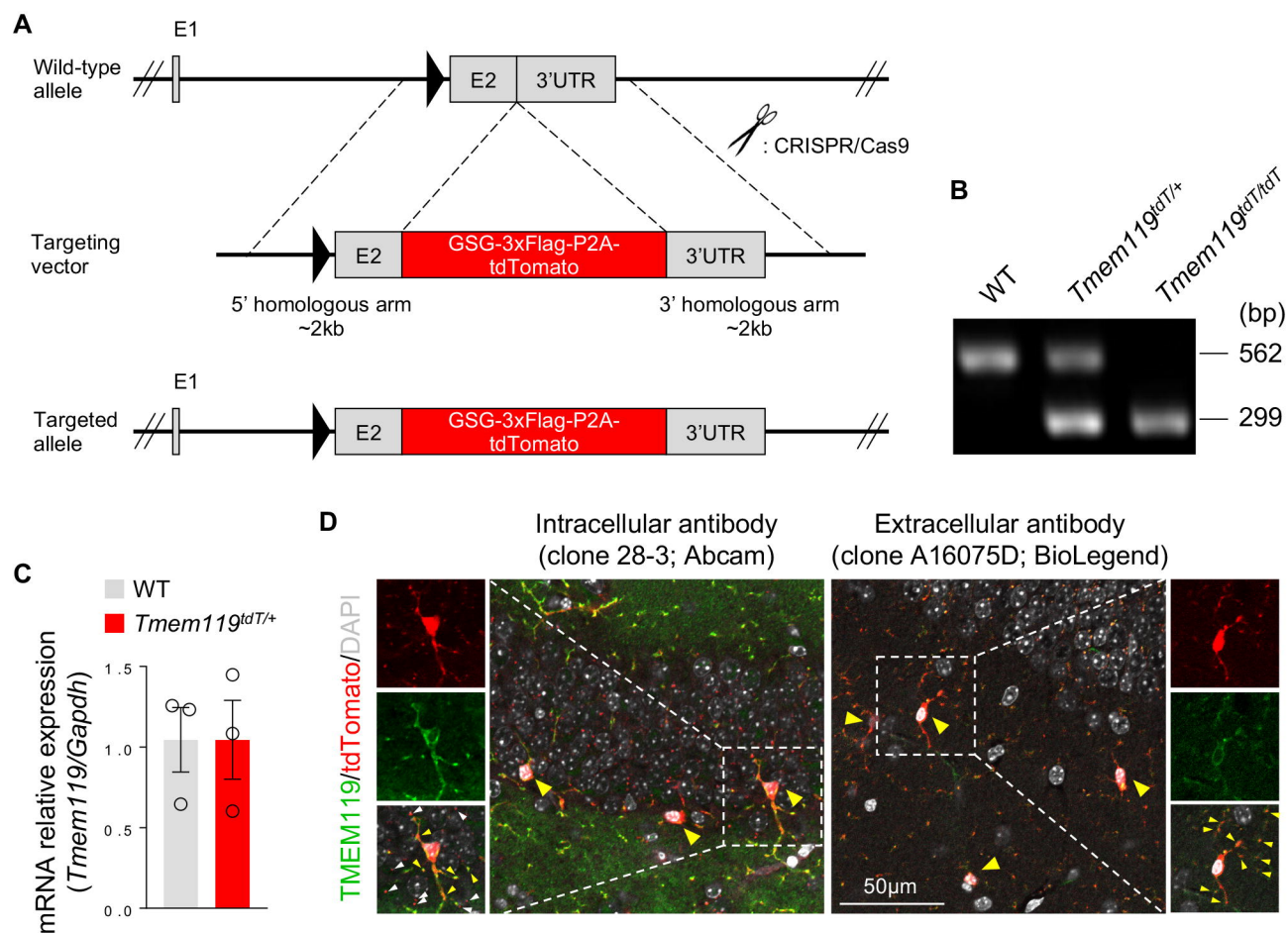601   **Supplementary data**

602   **Supplementary file 1: Detailed workflow for the design and the generation of the**

603   ***Tmem119-tdTomato* knock-in mice.** Five sections are provided to highlight the workflow of

604　the mouse generation starting from the targeting strategy using CRISPR/Cas9 technology, the

605　Cas9/sgRNA plasmid contruction and UCA assay, targeting vector construction & Southern

606　blot strategy design, sgRNA preparation, the zygote microinjection & founder genotyping.

607

608　**Supplementary file 2: Genotyping guide of the *Tmem119-tdTomato* knock-in mice.** This

609　report includes primer design strategy, primer sequences and predicted product sizes, PCR

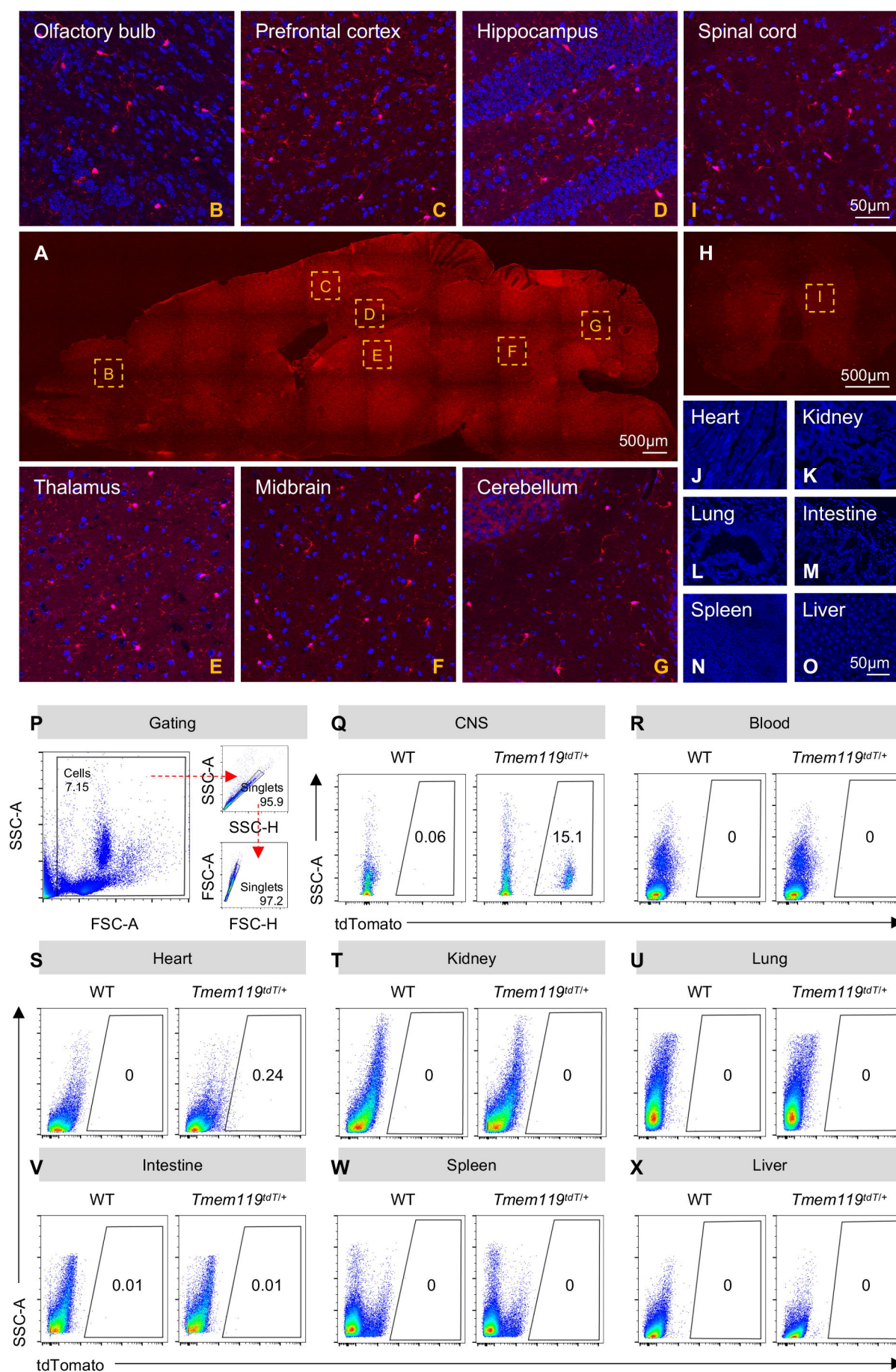610　reaction system & conditions, gel images, and determination of genotype from the gel image

611　results.

612

613　**Supplementary video: Time-lapse video of TMEM119-tdTomato$^+$ microglia response to**

614　**laser-induced injury.** After a localized ablation inside the primary sensory cortex,

615　neighboring tdTomato$^+$ microglia respond quickly with extended processes and bulbous
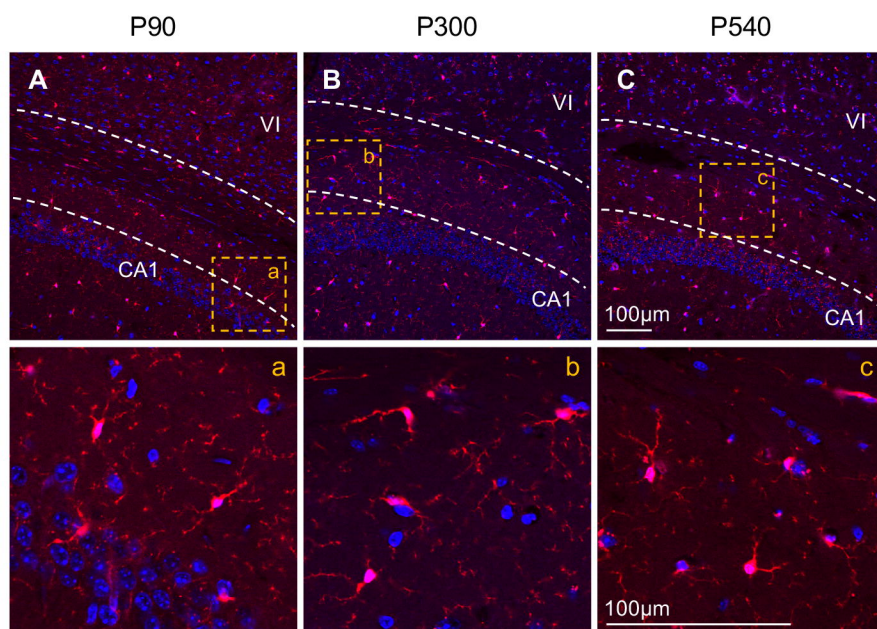
616　termini.

617

618

619

Figure 1

A

Wild-type allele

E1

Targeting vector

| E2 | GSG-3xFlag-P2A-tdTomato | 3'UTR |

5' homologous arm ~2kb

3' homologous arm ~2kb

✂ : CRISPR/Cas9

Targeted allele

E1

| E2 | GSG-3xFlag-P2A-tdTomato | 3'UTR |

B

WT $Tmem119^{tdT/+}$ $Tmem119^{tdT/tdT}$

(bp)

— 562

— 299

C

□ WT
■ $Tmem119^{tdT/+}$

mRNA relative expression ($Tmem119/Gapdh$)

1.5

1.0

0.5

0.0

D

TMEM119/tdTomato/DAPI

Intracellular antibody (clone 28-3; Abcam)
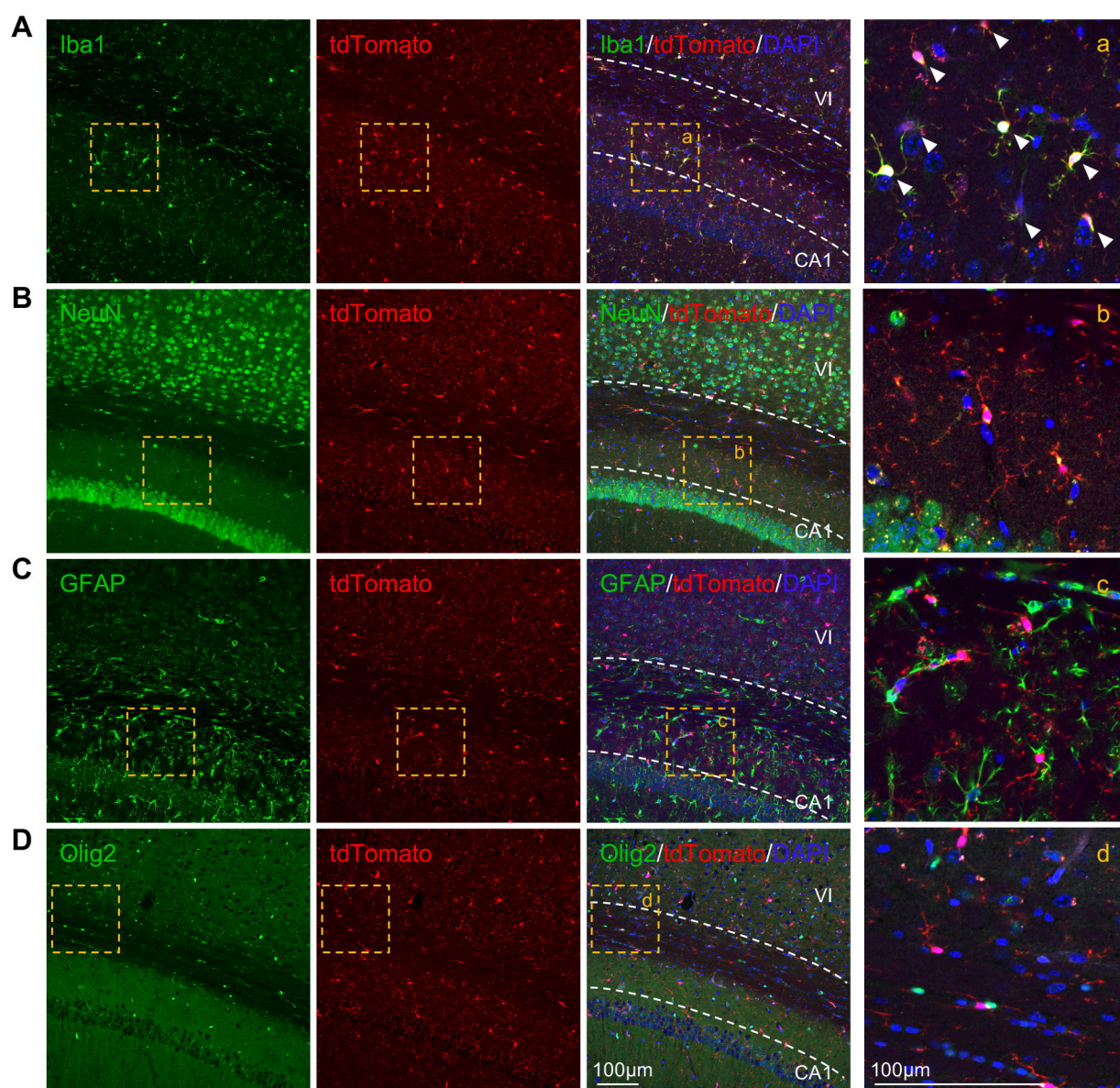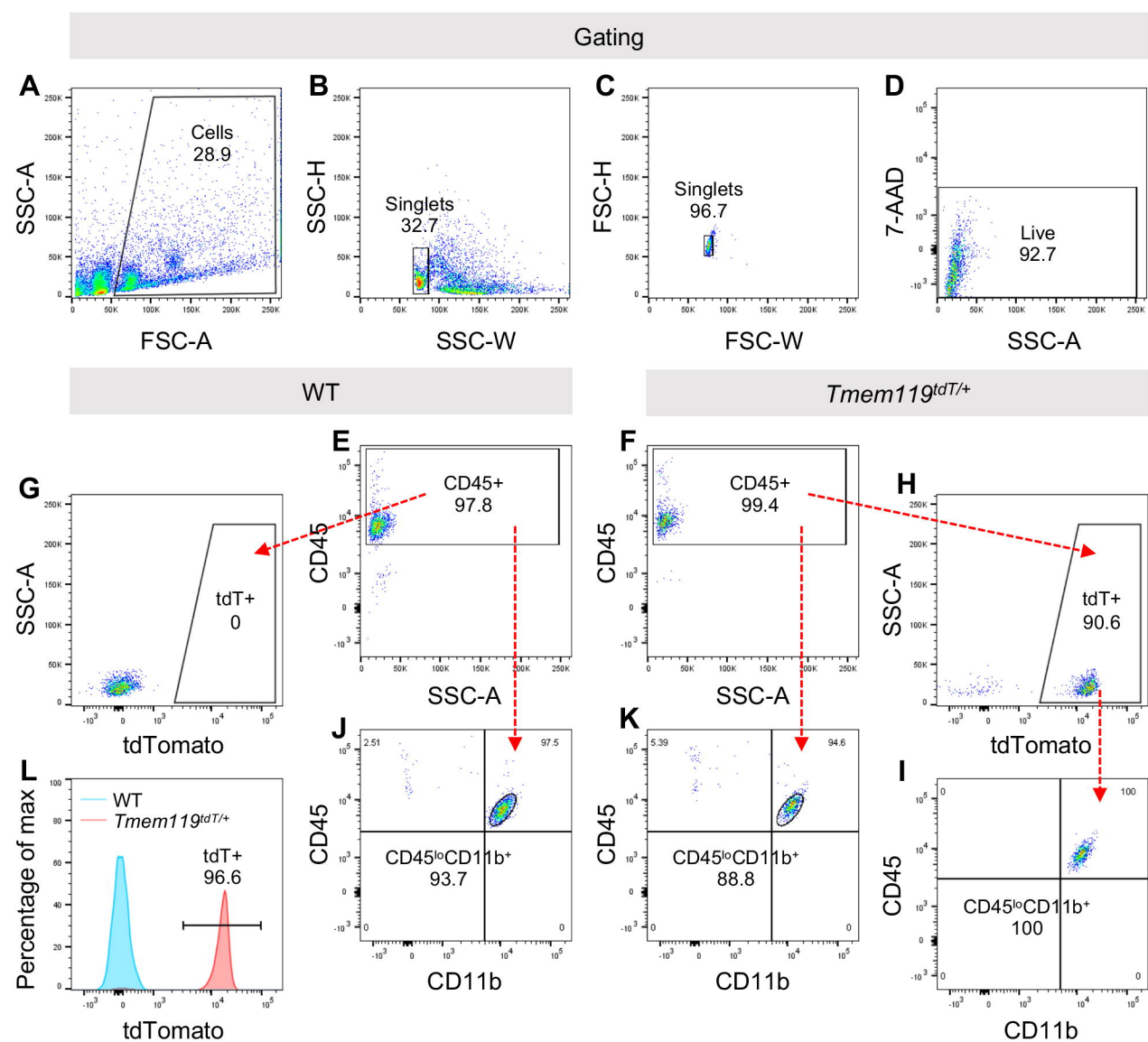
Extracellular antibody (clone A16075D; BioLegend)

50μm

Figure 2

Figure 3

Figure 4

Figure 5

Figure 6